Influence of the first wall material on the particle fuelling in ASDEX Upgrade

T. Lunt[1], F. Reimold[2], E. Wolfrum[1], D. Carralero[1], Y. Feng[3], K. Schmid[1], and the ASDEX Upgrade Team

[1] *Max Planck Institute for Plasma Physics, Boltzmannstr. 2, 85748 Garching, Germany*

[2] *Institut für Energie- und Klimaforschung - Plasmaphysik, Forschungszentrum Jülich GmbH, 52425 Jülich, Germany*

[3] *Max Planck Institute for Plasma Physics, Wendelsteinstr. 2, 17491 Greifswald, Germany*

Abstract

In the period from 2002 to 2007 the material of the plasma facing components (PFCs) of ASDEX Upgrade (AUG) was changed from carbon (C) to tungsten (W). Comparing the measured density profiles of low-density L-mode discharges with little or no gas puff before and after this modification, a significantly higher pedestal-top density was found for W PFCs together with a steeper gradient and a lower pedestal temperature. This change can be explained by larger particle- and energy reflection coefficients for D on W compared to D on C, as shown by EMC3-EIRENE simulations of AUG discharges in similar conditions on a computational grid extending to the main chamber first wall. In the simulations, a change of the wall material at fixed separatrix density indeed shows that for W PFCs more neutrals cross the separatrix, resulting in a steeper density gradient. Analysis of the source resolved and poloidally resolved neutral flux densities across the separatrix show a dominant contribution of the divertor targets to the fuelling profile in the simulation of the low density case. Increasing the density decreases the electron temperature at the target and therefore the potential drop in the electrostatic sheath as well as the energy of the ions impinging on the surface. Neutrals with ∼eV energies, able to reach the separatrix, are then only produced via molecular dissociation processes in the plasma volume independently of the PFC material. Also the contribution of the main chamber PFCs to the fuelling is observed to increase at higher densities.

1. Introduction

The performance of a fusion power plant depends – among other factors – on its plasma facing components (PFCs). In the past the PFCs in many tokamaks worldwide were preferentially made from low Z materials like carbon (C), as high Z materials can radiate large amounts of power in the confined region thereby cooling the plasma and reducing the performance of the device. However, carbon is not a viable material for the PFCs in ITER, because it can bind large amounts of tritium chemically, which would lead to an access of the permitted limits for the radioactive tritium inventory already after a few tens of discharges [1], while in a reactor the large erosion yield of C is likely prohibitive. The graphite and CFC (carbon fiber reinforced carbon) tiles in ASDEX Upgrade (AUG) were therefore gradually replaced by tungsten (W) PFCs in the period from 2003 to 2007 [2]. In JET the so-called ITER-like wall (ILW), with main chamber PFCs made from Beryllium and divertor tiles from W, was installed [3] and Alcator C-mod [4] and EAST (main chamber) [5] operate with PFCs from molybdenum.

Beneficial properties of the W PFCs are the reduced retention of hydrogenic species within the wall material as well as the lower sputtering yield and therefore low erosion rates. The much lower chemical reactivity of W compared to C avoids chemical sputtering [6] as well as co-deposition of hydrogenic species as layers

Email address: tilmann.lunt@ipp.mpg.de (T. Lunt[1])

	D→C			D→W		
$\mathbf{E_0}$	$\mathbf{R_N}$	$\mathbf{R_E}$	$\langle \mathbf{E} \rangle$	$\mathbf{R_N}$	$\mathbf{R_E}$	$\langle \mathbf{E} \rangle$
10 eV	0.4	0.13	2.5 eV	0.8	0.6	7.5 eV
20 eV	0.32	0.12	7.5 eV	0.71	0.52	14.6 eV
50 eV	0.3	0.1	16.6 eV	0.68	0.38	27.9 eV

Table 1: Particle and energy reflection coefficients, R_N and R_E, as well as mean energies $< E >$ for D ions at normal incidence ($\alpha = 0$) on C or W for three selected incident energies E_0

of hydrocarbons [7]. In addition, W has a higher reflection coefficient for impinging hydrognic ions [8], i.e. the probability that an impinging hydrogenic ion is directly reflected as a neutral, without being ad- or absorbed first, is higher. In contrast to thermally desorbed neutrals with energies of < 1 eV, reflected neutrals can carry a large fraction of the energy of the incident ions. With increasing energy the mean free path of neutrals and, hence, the probability to reach the confined plasma before being ionized increases. In particular in regions of low cross-field transport, such as the edge transport barrier, this local particle source can determine the shape of the density profile.
At AUG it was found that the power threshold for the transition from L- to H-mode (P_{thr}) was about 25% lower after completing the change to the full W wall and carefully cleaning all surfaces [9]. A detailed analysis of the edge density and temperature profiles showed that this decrease in P_{thr} could be attributed to the fact that the L-mode density profile has steeper gradients with W PFCs than with C PFCs, that enhance the critical flow shear [10] assumed to be necessary for the L-H transition.
The cause of the altered density profile shape was initially not completely clear. The production of large amounts of neutrals in the inner divertor in the early phase of the discharge was discussed as a possible explanation. However, the steeper edge electron density profiles were found even without these neutrals from the inner divertor. Another explanation relies on the different characteristics of the PFC materials, in particular the reflection coefficients. In this work we investigate the influence of the first wall material on the particle fueling. The paper is structured as follows: first, an overview of the particle and energy reflection from PFCs is presented (Sec. 2), and then we show experimental findings (Sec. 3), i.e. comparisons of edge density profiles in C and W PFCs from AUG. We report on EMC3-EIRENE simulations used to compute the transport in the bulk plasma, particle- and energy deposition profiles to PFCs in the divertor- and main chamber (MCPFCs) as well as the transport of neutral particles from these surfaces in Sec. 4. The impact of the divertor PFC material (C or W) and of that of the MCPFCs (W, C or Be) in particular on the electron density profile is studied. The results are summarized in Sec. 5.

2. Particle reflection from PFCs

An ion (projectile) incident on a PFC is scattered on the bulk material atoms (target) depending on the mass ratio of the collision partners and the angle of incidence. Under stationary conditions the net-flux of particles to the bulk must vanish, requireing 100% recycling (unless we are concerned with 'pumping' surfaces, that are not regarded here). Part of the particles are implanted in the bulk and are re-emitted later as thermal particles from the surface via out-diffusion and recombination, while another fraction $R_N(E_0, \alpha) = N/N_0$ is reflected directly. Following Ref. [11] N_0 is the number of projectiles at a given incidence energy E_0 and angle α and N that of the emitted particles independently of their energy, charge state or emission angle. Note that it is very likely (99 % for $E_0 < 500$ eV) that an incident ion is reflected back as a neutral atom as shown in Fig. 2.19 in Ref. [11]. Equivalently the energy reflection coefficient is defined as $R_E(E_0, \alpha) = \mathcal{E}/(E_0 N_0)$, where $\mathcal{E}$ is the sum over all backscattered particle energies independently of their charge state and emission angle. The mean energy of the reflected particles is then given by

$$\langle E \rangle (E_0, \alpha) = E_0 \frac{R_E (E_0, \alpha)}{R_N (E_0, \alpha)}. \quad (1)$$

Table 1 shows the values of R_N, R_E and $\langle E \rangle$ for Deuterium projectiles incident on C and W bulk material, for incidence energies of 10, 20 and 50 eV according to Ref. [8]. Older data can also be found in [11]. The mean incidence energy of ions after having fallen through the electrostatic sheath forming in front of a surface in contact with a plasma is given by $\langle E_0 \rangle = \gamma_i T_i + 3ZT_e$, where $\gamma_i = 2$ and $Z = 1$ for deuterium.
As can be seen from Tab. 1, not only the probability to be reflected from W is higher by a factor of 2 for a 10 eV incident D ion, but also the mean energy (7.5 eV) of the reflected atom is 3 times higher than that reflected from C (2.5 eV) for the same incidence energy. Moreover, this mean energy is higher than the energy of particles resulting from a molecular Franck-Condon decay ($\sim$ 2.5 eV) [12].
The values evaluated according to Ref. [8] stem from a comparison of experimental data with TRIM (transport of ions in matter) [13] calculations and a best fit through both. Experimentally determined reflection coefficients of D on C at various angles and fairly low energies can be found in Ref. [14]. An important result from these investigations is that TRIM calculations reproduce experimental data for smooth surfaces very well. Experimental measurements of H_a spectra in front of limiters with different mass (C and stainless steel) [15] confirm that the TRIM data allow a rather accurate simulation of the surface reflection. For rough surfaces the angle of incidence plays a crucial role and TRIM data might not be reliable. A direct comparison of a W and C limiter tile was carried out at the TEXTOR twin test limiter [16]. The spectroscopic investigation of radiation emitted by reflected D atoms as well as a 30 % reduction of the heat flux under similar plasma conditions were consistent with the higher reflection coefficients.
While at high energies TRIM calculations match experimental data quite well [8], and at very low energies molecular dynamic calculations confirm the extrapolated TRIM calculations, in the intermediate energy range 1 eV $< E_0 <$ 50 eV the TRIM calculations are the only data source. The TRIM data are the basis for the reflection coefficients implemented in the EIRENE package [17], which is used in the EMC3-EIRENE modelling presented in section 4.

3. Experimental findings

In Fig. 1 electron density (n_e) profiles of AUG L- and H-mode discharges with full W PFCs are compared to similar ones with C PFCs. General information about AUG can be found in Ref. [18] as well as the references therein. The n_e profiles are acquired with the lithium beam emission spectroscopy diagnostic (Li-BES) [19] and evaluated by modelling the collisional radiative occupation of the lithium atomic states within a Bayesian probability framework [20]. The temporal resolution of the n_e profile measurements is 1 ms.
The first two examples, shown in figure 1.a, are edge n_e profiles in low confinement mode (L-mode) at two different plasma currents, I_p = 0.8 and 1 MA, at toroidal magnetic field strengths between $B_t = -2$ and -2.2 T, with no gas puff. The uncertainty in the relative positioning is about 5 mm from the diagnostic spatial resolution plus another 5 mm stemming from the equilibrium reconstruction. Although the relative positioning could change due to these uncertainties, it is obvious that the density at $\rho_{pol} \sim 0.98$ is significantly lower for C PFCs compared to W PFCs for both plasma currents, 0.8 and 1 MA. Moreover, the gradients, averaged in the steep gradient region at $\rho_{pol} \sim 0.99$, are stronger in the W PFC cases. It is important to note that these profiles are established without gas puff. The steeper edge density gradients as well as shorter gradient lengths just inside the separatrix were identified as the cause for the lower power threshold for the transition from L- to H-mode in AUG with W PFCs as shown in Ref. [10], where a large number of discharges were analyzed.
When switching-on a strong gas puff, the electron density in the SOL rises and the divertor becomes more and more collisional. The collisionality in the divertor can lead to the formation of a so-called density shoulder, i.e. a region with a flat density profile (i.e. with a small gradient). The formation of this density shoulder was found to coincide with the occurrence of large filaments [21, 22], turbulent structures elongated along the field lines that might be responsible for an enhanced convective radial particle transport. Profiles of such discharges with W and C PFCs are compared in figure 1.b. Both discharges are ohmically heated, with I_p = 800 kA and $B_t = -2.5$ T. All available n_e profiles during a 40 ms period are plotted. In this case no difference in the density profiles can be seen.
The ion energy distribution function was measured at the outboard midplane by an $E \times B$ analyzer. In

Material divertor/MCPFCs	CX	R_N	n_{sep} [10^{19} m^{-3}]	Φ_{mc} [A]	Φ_{sep} [A]	Φ_{recyc} [A]	Φ_{mc}/Φ_{sep} [%]
W/W	1	$\neq 0$	0.8	227	357	5845	63.67
W/W	0	$\neq 0$	0.8	191	409	5845	46.80
C/C	1	$\neq 0$	0.8	175	301	6372	58.14
C/C	0	$\neq 0$	0.8	159	289	6372	55.08
C/C	1	0	0.8	143	222	7453	64.45
C/C	0	0	0.8	159	242	7453	65.81
W/C	1	$\neq 0$	0.8	197	394	5589	49.90
W/Be	1	$\neq 0$	0.8	201	399	5530	50.28
W/W	1	$\neq 0$	2.0	225	333	10776	67.64
W/W	0	$\neq 0$	2.0	221	424	10776	52.28
C/C	1	$\neq 0$	2.0	169	222	11177	76.08
C/C	0	$\neq 0$	2.0	168	228	11177	73.70
C/C	1	0	2.0	135	172	10825	78.32
C/C	0	0	2.0	155	176	10825	88.30

Table 2: Flux of neutrals Φ_{sep} over the entire separatrix and over its main chamber interval Φ_{mc}. Φ_{recyc} is the total recycling flux onto all PFCs. For some cases the reflection coefficient R_N was artificially set 0. For those cases all neutrals are released as thermal particles from the PFCs. For the underlined cases the source resolved fluxes are also given in Tab. 3

contrast to the case without density shoulder a large population of cold ions (< 10 eV) was found for the case with density shoulder indicating the occurrence of strong recycling [23]. Finally, Fig. 1.c shows examples of H-mode profiles from phases of similar discharges with the two different PFC materials without gas puffing. The discharges and profiles described earlier [24] are at $I_p = 1$ MA, $B_t = -2.5$ T, and have phases with different heating power. Solid- and dashed curves represent discharges with 8 and with 13 MW, respectively. Only profiles from the period -3 ms to -1 ms before an ELM are selected in a ~ 300 ms time interval with otherwise constant plasma parameters. At both heating powers the profiles with W PFCs reach higher pedestal top values. As was shown in Ref. [24], the electron temperature at the pedestal top is lower with W PFCs, leading to similar edge pressure profiles. Note that a contribution of impurity electrons to the n_e profile cannot explain the higher densities since the impurity concentration in the SOL with W PFCs is generally lower.
The peak target electron temperatures for the discharges shown in Fig. 1 are between 20 and 30 eV without gas puff (Fig. 1.a and Fig. 1.c) and below 7 eV with strong gas puff (Fig. 1.b). Apparently a material dependence of the density profile is only seen if the target electron temperature is high. Note that the equilibria corresponding to the profiles shown in Fig. 1 are not exactly equal.

4. Modelling

In order to test if the changes in the edge density profiles are predominantly due to an increased particle and energy reflection from the W PFCs, numerical modelling is necessary. Here, the neutral particle and plasma transport was studied by means of EMC3-EIRENE simulations. EMC3 solves Braginskii-like equations treating the plasma as a fluid. It is self-consistently coupled to the kinetic neutral transport code EIRENE [17]. The details of EMC3 and the coupling of the two codes, that both apply a Monte Carlo principle to solve the equations, are described in [25, 26]. The simulations are based on the AUG case labeled 'case B' in Ref. [27], where the magnetic equilibrium of discharge #29887 at 4.430 s was used. The computational grid extends radially until $\rho_{pol} = 1.15$, i.e. beyond the main chamber plasma facing components (MCPFCs) located at $\rho_{pol} = 1.038$ (inner heat shield) and $\rho = 1.05$ (ICRH limiters). Both, the flux of ions to the MCPFCs as well as the source of neutrals from that surfaces were taken into account in the

Source	$\Phi^i_{target}/\Phi_{recyc}$	$\Phi^n_{target}/\Phi_{sep}$
W div / W MCPFCs	$n_{sep} = 0.8 \times 10^{19}$ **m**$^{-3}$	
Inner target	39.2	34.2
Outer target	58.3	47.9
Limiters	2.4	17.4
Inner h.s.	0.1	0.9
C div / C MCPFCs	$n_{sep} = 0.8 \times 10^{19}$ **m**$^{-3}$	
Inner target	39.5	35.5
Outer target	58.4	49.9
Limiters	2.0	14.1
Inner h.s.	0.1	0.7
W div / W MCPFCs	$n_{sep} = 2.0 \times 10^{19}$ **m**$^{-3}$	
Inner target	40.5	22.8
Outer target	54.9	37.7
Limiters	4.3	36.8
Inner h.s.	0.2	2.2

Table 3: Source resolved particle fluxes. Φ^i_{target} is the ion flux to the individual targets that sum up to the total recycling flux $\Phi_{recyc} = \sum \Phi^i_{target}$ of ions to- (and of neutrals from) all PFCs. Φ^n_{target} is the separatrix flux of neutrals that originate from a specific target (not to be confused with the generally smaller flux of neutrals being emitted from that surfaces) that sum up to the total flux $\Phi_{sep} = \sum \Phi^n_{target}$ of neutrals across the separatrix.

simulation. In contrast to the simulation of case B in Ref. [27] but in order to match conditions similar to the cases shown in Fig. 1.a we assumed a much lower density $n_{sep} = 8 \cdot 10^{18}$ m^{-3} and a slightly higher input power $P_{in} = 800$ kW (equally distributed between the ions and the electrons) in this first set of simulations carried out in pure deuterium. Furthermore, diffusive transport coefficients $D_\perp = 0.1$ m^2/s in the core to $D_\perp = 0.9$ m^2/s in the SOL, with $\chi_\perp = 3D$ are assumed (i.e. as in 'case A' in Ref. [27]) to emulate a low-power, low-density L-mode discharge). For particles the computational domain is a closed system, i.e. ions fully recycle at the PFCs, neither external sources nor sinks in form of pumps are implemented. The same neutral particle reactions were used as in Ref. [28] except for volumetric recombination, a process not (yet) taken into account in EMC3-EIRENE, and (charge conserving) neutral-ion elastic collisions. A typical electron-, atomic-, and molecular density distribution in the poloidal plane at the toroidal angle Φ=11.25^o (center of Segment 1) is shown in Fig. 2 for the all-W PFC case. Note that the neutrals can also travel into the main chamber behind the divertor structures. This neutral flux is strongly determined by the size of the gaps on the HFS (21 mm), the LFS (17 mm) and below the divertor (26 mm).

Fig. 3 shows radial profiles of diffusive cross-field transport coefficients for particles $D_\perp$ and energy $\chi_\perp = 3D_\perp$, electron density n_e, electron temperature T_e and the ionization profile in the confined plasma predicted by EMC3-EIRENE for C and W as PFC material. In addition, a case with C PFCs and with only thermal desorption of neutrals, i.e. no reflection ($R_N = 0$), is also shown. While n_e, T_e and $D_\perp$ are given along a straight line at the outboard midplane (OMP), S_i is poloidally averaged in the confined region. The profiles show a significant dependence on the wall material, which is attributed to the enhanced reflection coefficients (cf. Sec. 2), the only parameter changed in the simulation. Fig. 3 d shows the (atomic plus twice the molecular) flux density of neutrals across the separatrix as a function of the poloidal angle with respect to that of the X-point $\theta - \theta_{xp}$. The largest neutral flux densities occur in the region around the X-point. A comparable distribution and absolute value of fluxes was found in Ref. [29]. We will refer to the fluxes within the dashed red vertical lines (that mark the upper edges θ_1 and θ_2 of the main divertor tile, cf. Fig. 2) as 'divertor fluxes' $\Phi_{div} = \int_{\phi=0}^{2\pi} \int_{\theta_1}^{\theta_2} \Gamma_D + 2\Gamma_{D_2} dA$, where dA is the separatrix surface element at the angles ϕ and θ. Although the flux densities are much smaller there, the neutral flux across the much larger 'main chamber' interval of the separatrix Φ_{mc}, marked by the red arrow, are of similar magnitude. This is also shown in table 2 where in addition the total separatrix flux $\Phi_{sep} = \Phi_{div} + \Phi_{mc}$ as well as the

total recycling flux Φ_{recyc} is given (note that for both the last closed flux surface as well as the plasma-wall interface the total flux of neutrals is opposite to the total flux of ions across these boundaries, $\Phi^i = -\Phi^n$). The value for the total flux Φ_{recyc} is determined by the separatrix density, which is kept constant during the EMC3-EIRENE iterations. It is noteworthy that more particles are necessary in the runs with C PFCs than in the ones with W PFCs, an indication that more neutrals are already ionized in the SOL in the C PFC cases. The ratio Φ_{mc}/Φ_{sep} shows that the neutrals which cross the separatrix stem to about equal parts from the divertor and the main chamber regions. Note that this does *not* mean that all the main chamber neutrals originate from recycling at the limiters. A large fraction of these neutrals were emitted by the divertor targets and make their way into the main chamber using the sub-divertor by-passes.
On the converged solution for the plasma and the neutral sources EIRENE was run stand-alone with charge exchange (CX) processes turned off. The impact on the ionization profile as well as on the neutral flux across the separatrix are shown by the dashed lines in Figs. 3 b and d and in Tab. 2. Interestingly CX reduces the neutral flux across the separatrix Φ_{sep}, which is attributed to the isotropic scattering of neutrals that were moving towards the separatrix before the CX process. Apparently, this effect is larger than the gain of mean free path due to the (typically) higher energy after the CX-collision.
In another series of simulations (cf. figure 4) the divertor material is kept the same (W) while changing the MCPFCs. The fact that the profiles look very similar confirms that the fuelling is mainly caused by the divertor neutrals, and that the different materials of the MCPFCs do not play a significant role under these low density conditions.

However, when increasing the density in the simulation while keeping constant the heating power the electron temperature in the divertor and consequently the mean energy of the reflected particles strongly decreases. Neutrals with 2 to 3 eV energy are then produced via molecular dissociation processes in the plasma volume independently of the PFC material. The density profile in the SOL then look very similar for the different PFC materials. Furthermore, the recycled neutrals from the MCPFCs, due to their proximity to the separatrix, start to contribute significantly (37%) to the fuelling as seen in particular in Tab. 3. This explains the cold ion population mentioned in Sec. 3. However, the simulations at higher densities are associated with a rather high degree of uncertainty because the electron temperature in the divertor becomes so small that significant volumetric recombination is expected to set in, a process not taken into account in the simulation. Experimentally, however, the contribution of the MCPFCs might still be higher due to the aforementioned shoulder formation.

5. Summary

The particle- and energy reflection of impinging deuterium ions from a W plasma facing component (PFC) are considerably higher than those from a C PFC. This leads to a changed velocity distribution of recycled deuterium neutral atoms towards higher velocity components, because more particles are directly reflected as neutrals rather than thermally emitted. The effect as well as its impact on the plasma background is modelled by EMC3-EIRENE that is run on a computational grid extending to the first wall, so that the influence of all different PFCs, i.e. divertor and main chamber plasma facing components (MCPFCs), can be assessed simultaneously. The EIRENE code contains reflection data for various PFC materials, which stem from TRIM calculations. These data are experimentally verified at high energies (> 100 eV), but only extrapolated towards lower energies. A detailed comparison of experimental data in the relevant energy range from 1 eV to 100 eV is not available. Together with the undetermined surface roughness, which is known to play a crucial role for the actual reflection cross sections, the underlying data have considerable uncertainties. Nevertheless, the data is the best available, the uncertainties apply to all PFC materials and will affect mainly the absolute numbers, but not so much the difference between C and W.
An L-mode discharge with no gas puffing, in which only the PFC material was changed while keeping constant the density at the separatrix and the transport coefficients was simulated. The comparison of pure W PFCs with C PFCs shows that the ionization source profile inside the separatrix is higher in the W case, giving rise to an increased density with steeper gradients in that region. This is in qualitative agreement with the experimental profiles obtained in ASDEX Upgrade. Also the material mix W divertor/ Be MCPFCs, such as it is implemented in the JET ILW, as well as W divertor / C MCPFCs showed a steeper density

gradient compared to a pure C machine, because most of the neutral particles stem from the divertor region for these low density conditions.
A simulation with a higher separatrix density and the same input power shows that the effect is considerably reduced, because the electron temperature in the divertor and consequently the energy of the reflected particles become small such that the dominant process to produce neutrals in the ∼eV range is molecular dissociation. The contribution of neutrals reflected on the MCPFCs (limiters) to the total flux of neutrals across the separatrix can then become of the same order as those from the divertor targets. However, the simulations at high density are associated with a large uncertainty because the electron temperature in the divertor becomes so small that volumetric recombination would become important, a process not taken into account in the simulation.
Nevertheless, the experimental profiles shown in Fig. 1 can well be explained by the dependence of the particle reflection on the target material.

6. References

[1] Roth J. *et al.* 2009 *J. Nucl. Mat.* **390–391** 1–9
[2] Neu R. *et al.* 2007 *J. Nucl. Mat.* **367** 1497–1502
[3] Brezinsek S. *et al.* 2013 *Nucl. Fusion* **53** 083023
[4] Hutchinson I. H. *et al.* 1994 *Physics of Plasmas* **1** 1511
[5] Liu Z. X. *et al.* 2013 *Nucl. Fusion* **53** 073041
[6] Behrisch R. & Eckstein W., 2007 *Sputtering by Particle Bombardement, Topics in Applied Phyics Vol. 110, Springer, Berlin, Germany*
[7] Rohde V. *et al.* 2001 *J. Nucl. Mat.* **290–293** 317–320
[8] Eckstein W. 2009 *Reflection (Backscattering), Report IPP 17/12, IPP Garching*
[9] Ryter F. *et al.* 2013 *Nucl. Fusion* **53** 113003
[10] Shao L. *et al.* 2016 *Plasma Phys. Control. Fusion* **58** 025004
[11] Eckstein W., Verbeek H. 1984 *Nucl. Fusion* **24** S9 chapter 2
[12] Herzberg G. Monfils A. 1960 *J. Molec. Spectr.* **5** 482–498
[13] Biersack J.P. and Haggmark L.G. 1980 *Nucl. Instr. Meth.* **174** 257–269
[14] Mayer M. *et al.* 1995 *J. Appl. Phys.* **77** 6609–6615
[15] Reiter D. *et al.* 1992 *J. Nucl. Mat.* **196–198** 1059–1064
[16] Huber A. *et al.* 2001 *J. Nucl. Mat.* **290–393** 276–280
[17] Reiter D. *et al.* 2005 *Fus. Sci. Tec.* **47** 172–186
[18] Kallenbach A. *et al.* 2012 *IEEE Transactions on Plasma Science* **40** 605
[19] Wolfrum E. *et al.* 1993 *Rev. Sci. Instr.* **64** 2285–2292
[20] Fischer R. *et al.* 2008 *Plasma Phys. Control. Fusion* **50** 085009
[21] Carralero D. *et al.* 2014 *Nucl. Fusion* **54** 123005
[22] Carralero D. *et al.* 2015 *Phys. Rev. Lett.* **115** 215002
[23] Carralero D. *et al.* 2015 *EPS Conf. on Plasma Physics (2015), Lisbon, Portugal, O2.106*
[24] Schneider P.A. *et al.* 2015 *Plasma Phys. Control. Fusion* **57** 014029
[25] Feng Y. *et al.* 2004 *Contrib. Plasma Phys.* **44** No. 1–3, 57–69
[26] Feng Y. *et al.* 2014 *Contrib. Plasma Phys.* **54** No. 4–6, 426–431
[27] Lunt T. *et al.* 2015 *J. Nucl. Mater.* **463** 744–747
[28] Kotov V. *et al.* 2008 *Plasma Phys. Control. Fusion* **50** 105012
[29] Groth M. *et al.* 2011 *Plasma Phys. Control. Fusion* **53** 124017

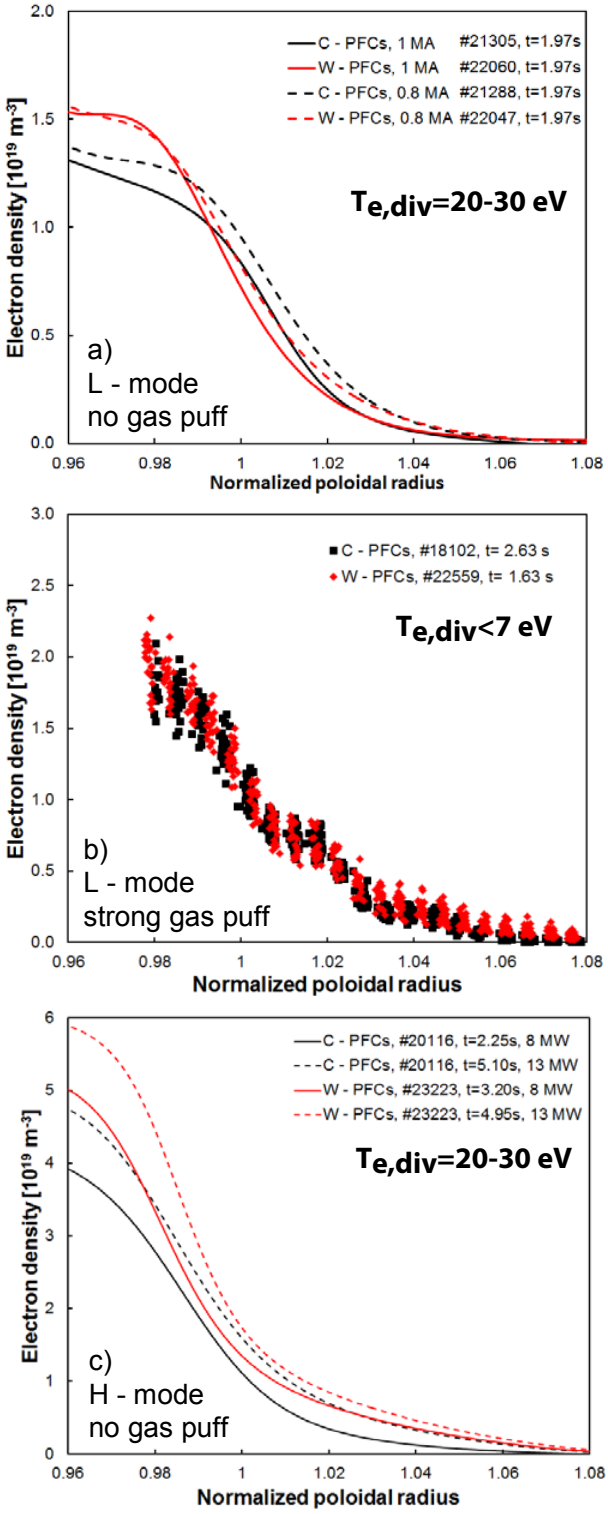

Figure 1: Density profiles in ASDEX Upgrade before and after the change from a C (black) to a W (red) wall. a) L-modes without fuelling at two currents, I_P = 800 kA (dashed lines) and 1 MA (solid lines). b) L-mode with strong fuelling. c) H-modes without fuelling at two different heating powers, 8 MW (solid lines) and 13 MW (dashed lines).

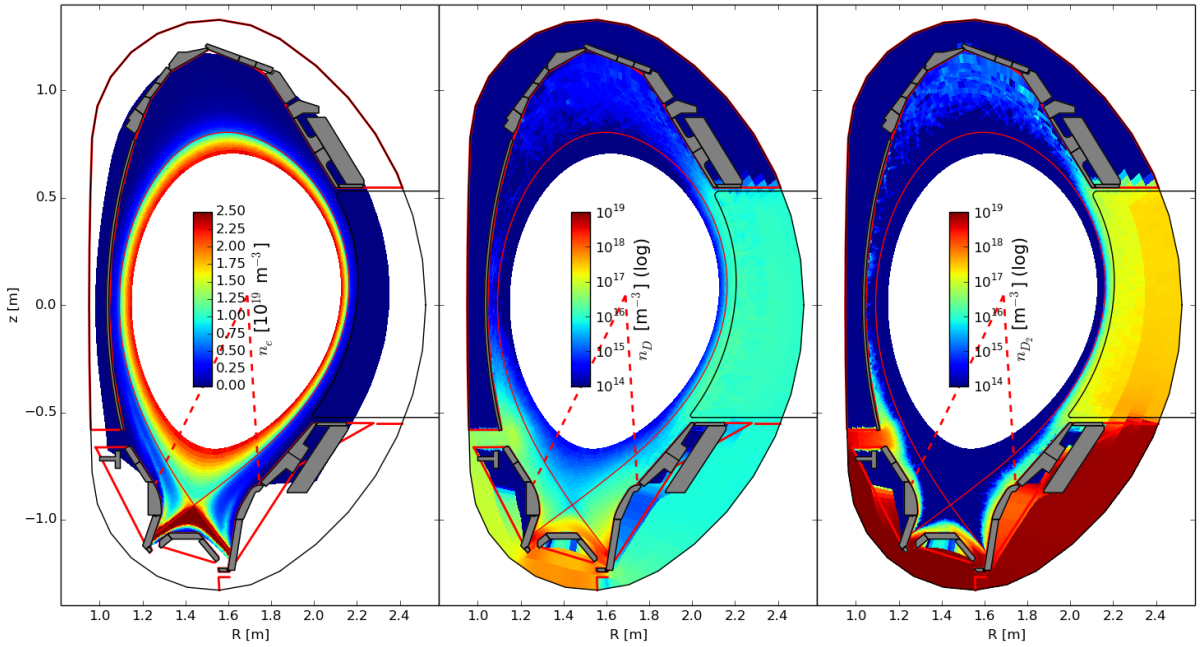

Figure 2: 2D profiles of electron- (left), neutral atom- (middle) and neutral molecular (right) density calculated by EMC3-EIRENE.

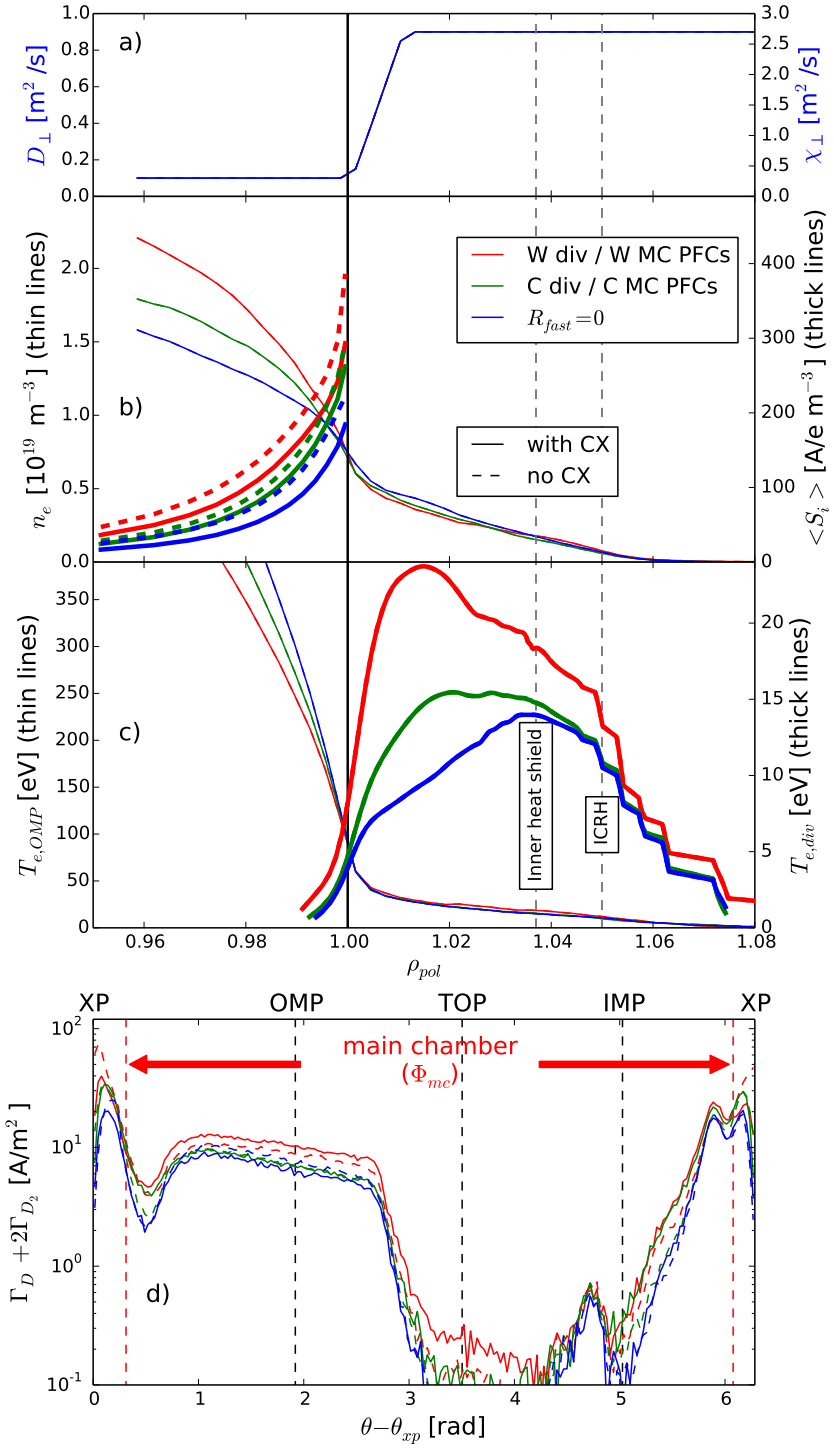

Figure 3: a) diffusive transport coefficients $D_\perp$ and $\chi_\perp = 3D_\perp$, b) outboard midplane density- (thin lines) and poloidally averaged ionization (thick lines) profiles, c) outboard midplane- (thin lines) and target electron temperature, d) total (atomic + molecular) neutral flux across the separatrix as a function of the poloidal angle θ, relative to that of the X-point, θ_{XP}. The line color indicates the material of the PFCs in both, the divertor and the main chamber.

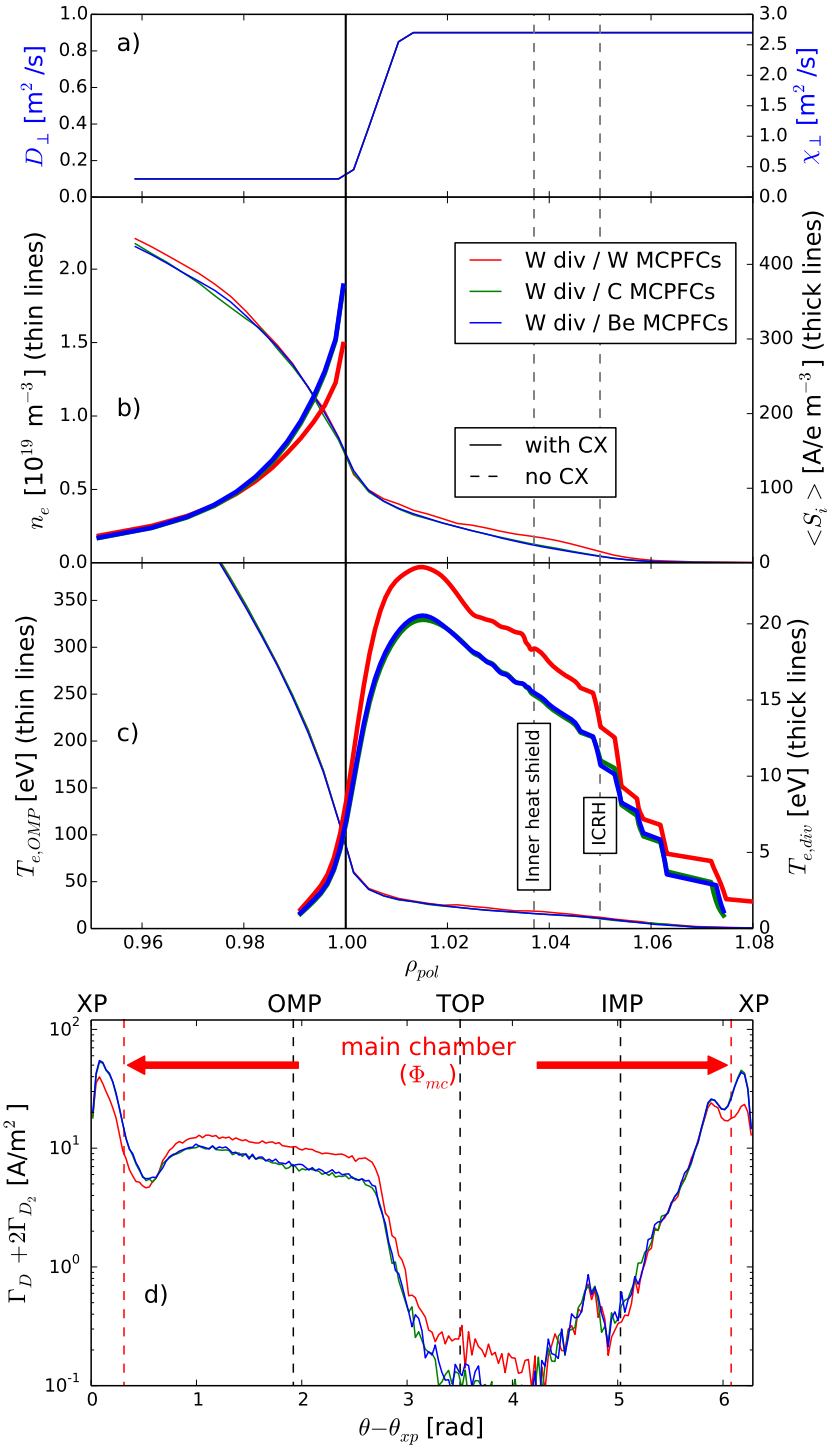

Figure 4: The same as in Fig. 3 but with W divertor PFCs and varying MC PFC materials.

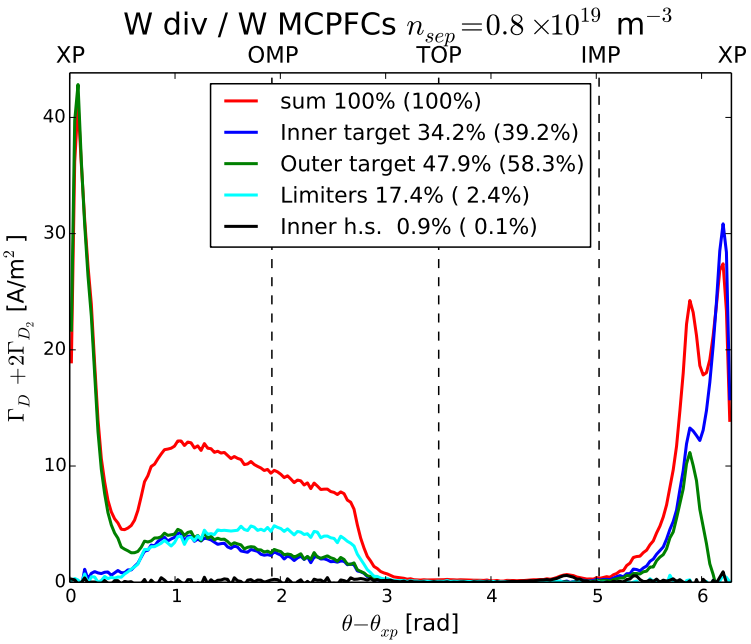

Figure 5: Source resolved contributions to the neutral flux across the separatrix.